Altered excitation energy transfer between phycobilisome and photosystems in the absence of ApcG, a small linker peptide, in Synechocystis sp. PCC 6803, a cyanobacterium

Rupal Singh Tomar, Dariusz M. Niedzwiedzki, Haijun Liu

PII: S0005-2728(24)00019-7

DOI: https://doi.org/10.1016/j.bbabio.2024.149049

Reference: BBABIO 149049

To appear in: *BBA - Bioenergetics*

Received date: 26 March 2024

Revised date: 14 May 2024

Accepted date: 21 May 2024

Please cite this article as: R.S. Tomar, D.M. Niedzwiedzki and H. Liu, Altered excitation energy transfer between phycobilisome and photosystems in the absence of ApcG, a small linker peptide, in Synechocystis sp. PCC 6803, a cyanobacterium, *BBA - Bioenergetics* (2023), https://doi.org/10.1016/j.bbabio.2024.149049

Altered Excitation Energy Transfer Between Phycobilisome and Photosystems in the Absence of ApcG, a Small Linker Peptide, in *Synechocystis* sp. PCC 6803, a Cyanobacterium

Rupal Singh Tomar[a], Dariusz M. Niedzwiedzki[b,c,*], Haijun Liu[a,*]

[a]Department of Biology, Saint Louis University, St. Louis, MO 63103, USA
[b]Center for Solar Energy and Energy Storage, Washington University in St. Louis, St. Louis, MO 63130, USA
[c]Department of Energy Environmental and Chemical Engineering, Washington University in St. Louis, St. Louis, MO 63130, USA

**Corresponding authors' emails:*

Dariusz M. Niedzwiedzki: niedzwiedzki@wustl.edu

Haijun Liu: haijun.liu@slu.edu

Highlights

- Time-resolved fluorescence unveiled the photophysical characteristics of ΔApcG-PBS.
- Mutation induces very minor disruptions within the allophycocyanin (APC) core.
- Distinct spectral subgroups of short-lived APC identified in ΔApcG-PBS.
- Small linker protein causes altered energy transfer from PBS to RC
- Deletion of ApcG subunit does not impede state transitions in mutant cells.

Abstract

Phycobilisome (PBS) is a large pigment-protein complex in cyanobacteria and red algae responsible for capturing sunlight and transferring its energy to photosystems (PS). Spectroscopic and structural properties of various PBSs have been widely studied, however, the nature of so-called complex-complex interactions between PBS and PSs remains much less explored. In this work, we have investigated the function of a newly identified PBS linker protein, ApcG, some domain of which, together with a loop region (PB-loop in ApcE), is

possibly located near the PBS-PS interface. Using *Synechocystis* sp. PCC 6803, we generated an ApcG deletion mutant and probed its deletion effect on the energetic coupling between PBS and photosystems. Steady-state and time-resolved spectroscopic characterization of the purified ΔApcG-PBS demonstrated that ApcG removal weakly affects the photophysical properties of PBS for which the spectroscopic properties of terminal energy emitters are comparable to those of PBS from wild-type strain. However, analysis of fluorescence decay imaging datasets reveals that ApcG deletion induces disruptions within the allophycocyanin (APC) core, resulting in the emergence (splitting) of two spectrally diverse subgroups with some short-lived APC. Profound spectroscopic changes of the whole ΔApcG mutant cell, however, emerge during state transition, a dynamic process of light scheme adaptation. The mutant cells in State I show a substantial increase in PBS-related fluorescence. On the other hand, global analysis of time-resolved fluorescence demonstrates that in general ApcG deletion does not alter or inhibit state transitions interpreted in terms of the changes of the PSII and PSI fluorescence emission intensity. The results revealed yet–to–be discovered mechanism of ApcG-docking induced excitation energy transfer regulation within PBS or to Photosystems.

Key words: phycobilisome, ApcG, the core-membrane linker (Lcm), excitation energy transfer, spectroscopy, time-resolved fluorescence, phycobilisome-RC interface.

1. Introduction

Cyanobacteria are prokaryotic photosynthetic organisms engaged in oxygenic photosynthesis and present across diverse ecological habitats [1, 2]. In cyanobacteria and red algae, the key role in light harvesting is undertaken by phycobilisomes (PBSs), extrinsic complexes comprising multiple pigmented and pigment-free proteins. PBSs are intricately associated with the cytoplasmic side of the thylakoid membrane [3, 4]. The major components of PBS (~85%) are phycobiliproteins (PBPs), containing colored pigments (phycocyanobilins, PCBs) and the remaining ~15% correspond to colorless linker proteins [5, 6]. PBS is comprised of numerous units featuring the PBPs phycocyanin (PC) and allophycocyanin (APC) and adopts various configuration [5]. APC forms the central core, functioning as a structural framework for the attachment of outward-extending PC rods, and relays the excitation energy from the PC rods to the photosystems (PS). These rods are constructed from stacked discs, each comprising six α/β

PC heterodimers and associated linker proteins. In PBS from *Synechocystis* sp. PCC 6803 (hereafter, *Synechocystis* 6803) the central core comprises three cylinders (so-called tricylindrical PBS), each housing four stacked APC discs (**Figure 1**). Nevertheless, considerable variations exist in the organization and composition of PBS, based on the species and prevailing growth conditions [7]. PBPs play a crucial role in capturing and transferring light energy, while linkers contribute to the accurate assembly of PBS and fine-tune the energy transfer within PBS components and between PBS and PS [8, 9].

In *Synechocystis* 6803, the two basal cylinders parallel to the thylakoid membrane along with the APC variants ApcD and ApcF consist of the core membrane linker L_{CM} (ApcE) (**Figure 1B**). These APC subunits play a crucial role in facilitating energy transfer to the respective photosystems. ApcE, in addition to its scaffolding function of stitching three cylinders together using its linker domain [10-12], is specifically implicated in transferring energy to PSII using a terminal energy emitter (located in the phycocyanobilin domain or PB domain) while ApcD and ApcF are suggested to function primarily as excitation energy donors for PSI [13-15]. Recent elucidations of the PBS structure in both, red algae and cyanobacteria, using cryogenic electron microscopy (cryo-EM) have greatly advanced our understanding of this remarkable pigment protein complex [9, 16, 17]. Particularly in *Synechocystis* 6803, diverse rod conformations were unveiled and a newly identified PBS linker protein ApcG (sll1873) was discovered [17]. The C-terminal domain (CTD) of ApcG is situated within the two basal cylinders of the tri-cylindrical PBS core(**Figure 1B**) [17]. Our recent study, employing structural mass spectrometry techniques, uncovered the close spatial relationship between the PB-loop (an intrinsically disordered region, or IDR, within the PB domain) of ApcE and ApcG-CTD and proposed that the PB-loop and ApcG collectively form a structural protrusion towards the thylakoids [18]. Considering the core-membrane (PBS core and thylakoid membrane) and location of ApcG it could be hypothesized that the above-mentioned structural protrusion engages in the interactions with PS, potentially facilitate anchoring of PBS to the thylakoid membrane and integrate the cellular cues to regulate excitation energy transfer from PBS to RCs. A recent investigation demonstrated that ApcG exhibits specific binding to PSII through its N-terminal region, and this interaction is influenced by the phosphorylation status of ApcG [19]. Note that phosphorylation of ApcG (then unknown *Sll1873*) was reported in a previous photoproteome survey using LC-MS/MS [20]. Under normal light conditions, ΔApcG mutant cells displayed normal growth,

however, and exhibited slower growth compared to the wild-type (WT) under light-limiting conditions [19]. Analysis using low-temperature fluorescence revealed an imbalance in the activity of PSII and PSI in the mutant strain. The investigations strongly suggested that ApcG plays a crucial role in the interaction between the PBS and PSII, facilitating energy transfer towards PSI, likely through the spillover mechanism [19].

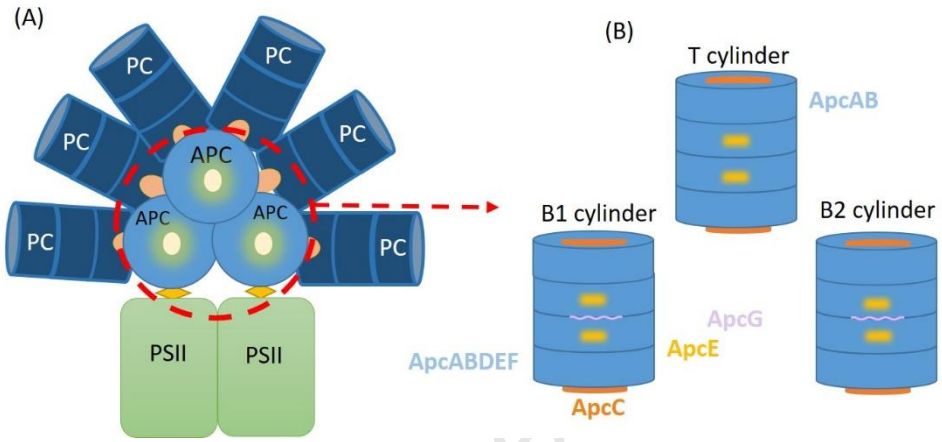

Figure 1. **Interaction of PBS with PSII**. (**A**) A cartoon model of PBS-PSII megacomplex. (**B**) Schematic overview of three PBS core cylinders. Location of ApcG linker protein indicated by violet ribbon; PC – phycocyanin, APC – allophycocyanin, PSII – photosystem II.

In this study, to assess the impact of ApcG on the structure and functionality of PBS, we generated a mutant strain in *Synechocystis* 6803 lacking ApcG (ΔApcG mutant). Our objective was to comprehensively analyze the deletion impact of ApcG on excitation energy transfer within PBS and from PBS to PSs. We have applied time-resolved spectroscopies such as fluorescence decay imaging and transient absorption on biochemically purified PBS samples as well as on the whole cells. The studies were performed in physiologically relevant temperature (room temperature) and at 77 K.

2. Materials and methods

2.1. Mutant construction

To create the ΔApcG mutant, a deletion plasmid was constructed by replacing partial *apcG* locus *(sll1873*) with a kanamycin (Km) resistance cassette (**Figure 2**).

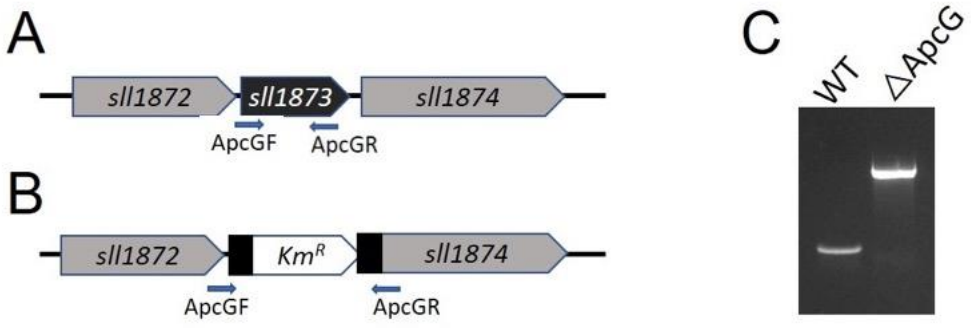

Figure 2. Construction of *ΔapcG* mutant. (**A**) *apcG* locus in *Synechocystis* 6803. (**B**) *apcG* deletion construct with a Kanamycin (Km) resistance cassette insertion. Primer pair ApcGF and ApcGR (Table S1) was used for the segregation analysis. (**C**) PCR segregation analysis of WT *Synechocystis* 6803 and ΔApcG mutant strains using primers in B (dark blue arrows).

ΔApcG_Km gene gBlock ordered from IDT (Coralville, IA, USA) was amplified by PCR using Q5 master mix (NEB, Ipswich, MA, USA) with Fw: pUCApcGF and Rev: pUCApcGR primers (Table S1). The purified PCR product of DNA was cloned into the linearized pUC19 vector (*Sma*I) by using NEBuilder HiFi DNA assembly master mix (NEB, Ipswich, MA, USA). 2 µL of assembly reaction was used for transformation into NEB 5-alpha competent *E. coli* cells (NEB#C2987, NEB, Ipswich, MA, USA). Recombinant cells were grown into LB agar plates containing 20 µg mL^{-1} of Km. Screening of positive transformants was done using colony PCR (Promega GoTaq master, Promega, Madison, WI, USA) with primers specific for the flanking regions Fw: M13Forward and Rev: KanNF (Table S1). Plasmid DNA was extracted using GeneJet mini plasmid kit (Thermo Fisher Scientific, Waltham, MA, USA). The construct sequence was confirmed by sequencing service from Genewiz or Azenta Life Science (South Plainfield, NJ, USA) using primers Fw: OCPKanF and Rev: KanCassR (Table S1) and analyzed with SnapGene software to confirm the mutations. The fresh WT cells of *Synechocystis* 6803 were then transformed with a recombinant plasmid carrying the ΔApcG gene to yield Km^R clones. The transgenic colonies appeared after two weeks were re-streaked on BG-11 plates with 20 µg mL^{-1} Km before liquid sub-culture and segregation analysis using primers specific for the flanking regions of deletion, Fw: ApcGF and Rev: ApcGR (Table S1). All primer sequences are listed in Table S1.

2.2. Growth of Synechocystis sp. PCC 6803 Strains

Synechocystis 6803 (WT) and ΔApcG strains were grown in BG11 medium [21] at 30 °C under white light condition of 30 µmol photons m^{-2} s^{-1}. ΔApcG mutant strain was grown in BG11 supplemented with antibiotic (Km, 20 µg mL^{-1}). Cultures were grown in a 3 L glass jars with air bubbling from the top. Cells in the late exponential growth phase were harvested by centrifugation (5000×g) and stored at -80 °C until further use.

2.3. Isolation of phycobilisomes

Phycobilisomes (PBS) were isolated as described previously [22, 23]. In brief, the harvested cell cultures from WT and ΔApcG mutant of *Synechocystis* 6803 were resuspended in 0.8 M K-phosphate (pH 7.5) buffer with protease inhibitor cocktail tablet (Thermo Fisher Scientific, Waltham, MA, USA) and pinch of deoxyribonuclease (DNase I) crystals (MilliporeSigma, Burlington, MA, USA). Cell lysates were obtained through three rounds of a French press cylinder prechilled at 4 °C. 20% (w/v) stock Triton X-100 (MilliporeSigma, Burlington, MA, USA) was then added drop by drop to a final concentration of 2%, followed by 30 min incubation at room temperature in the dark with gentle stirring. Samples were centrifuged at 25,000×g for 30 min at 4 °C. The blue supernatant below the top sticky lipid layer was loaded onto a sucrose gradient (0.25, 0.5, 0.75, 1 and 2 M sucrose in 0.8 M K-phosphate buffer, pH 7.5) for overnight ultracentrifugation (175,000×g). Blue bands of PBS at the interface of 0.75 to 1.0 M sucrose were collected and used for spectroscopic studies within a week from preparation.

2.4. Steady state spectroscopic characterization and sample handling

Steady state absorption of samples was recorded using UV-Vis 1800 spectrophotometer (Shimadzu, Kyoto, Japan). Cryogenic measurements were performed in the liquid nitrogen vapor-based VNF-100 cryostat (Janis Research, Woburn, MA, USA). Expected steady-state fluorescence emission spectra were obtained by time integration of time-resolved fluorescence emission contours (*vide infra*). All experiments were performed within two days from sample preparation.

2.5. Generation of state transitions in cyanobacteria whole cells

The state transitions in cells of WT and ΔApcG mutant of *Synechocystis* 6803 were studied at 77 K under the PBS excitation at 610 nm and under PSII/PSI excitation at 410 nm.

First, each liquid fresh sample was split into two identical batches. First sample batch was dark-adapted for 20 min at room temperature, placed in cryostat in dark and then slowly frozen in liquid nitrogen vapor (no flash freezing) to generate State II and conduct fluorescence emission studies. To generate State I, the second batch was dark-adapted for 20 min at room temperature, subsequently DCMU was added to a final concentration of 10 μM, sample was placed inside cryostat at room temperature, exposed to the far-red light (LED peaking at 730 nm wavelength to selective excite PSI) for 5 min and slowly, with light on, frozen in liquid nitrogen vapor.

2.6. Time-resolved fluorescence spectroscopy

Time-resolved fluorescence (TRF) experiments were conducted with streak camera system (a Hamamatsu, Japan) described in detail previously[24]. The samples were excited with ultrafast optical parametric oscillator (Inspire100, Spectra-Physics, Milpitas, CA, USA) pumped with ultrafast Ti:Sapphire laser (~90 fs duration at 820 nm, 80 MHz frequency) (Mai-Tai, Spectra-Physics, Milpitas, CA, USA). Excitation wavelength was set to 610 nm to preferentially excite blue edge of PBS absorption band. Before sampling, excitation beam frequency was lowered to 8 MHz (125 ns between subsequent excitations) with pulse selector (Pulse Selector model 3980, Spectra-Physics, Milpitas, CA, USA). Excitation power was adjusted to ~100 mW and focused on the sample in a circular spot of ~1 mm diameter corresponding to ~5×10^{12} photons cm^{-2} (laser fluence of ~16 nJ cm^{-2}).

2.7. Femtosecond time-resolved transient absorption spectroscopy

Time-resolved pump-probe transient absorption (TA) measurements were carried out using Helios, a femtosecond transient absorption spectrometer (Ultrafast Systems, Sarasota, FL, USA) coupled to a femtosecond laser system described previously [25]. All TA experiments were conducted at room temperature (293 K) for PBS samples placed in 2 mm path quartz cuvette. The samples excited at 590 nm, corresponding to the blue edge of PBS absorption band. The energy of the pump beam (of 1 kHz frequency) was set to 40 nJ in a spot size of ~1 mm diameter, corresponding to ~2×10^{13} photons cm^{-2} (laser fluence of ~50 nJ cm^{-2})

2.8. Spectroscopic data processing and global analysis

Dispersion present in the TA datasets was corrected using Surface Xplorer 4 (Ultrafast Systems, Sarasota, FL, USA). Global fitting of TRF and TA datasets was performed using

CarpetView (Light Conversion, Vilnius, Lithuania) with a fitting model assuming a sequential decay pathway of excitation energy [26] and in some cases with parallel decay model (simultaneous excitation and independent decay of all components). The fitting included convolution of the data with Gaussian-like instrument response function (IRF) having the full width at half maximum of ~200 fs for Helios (TA) and ~0.3 ns for streak camera setup (TRF). To clearly distinguish global analysis results of TRF and TA data the following terms were used: EAFS – evolution associated fluorescence spectra and DAFS – decay associated fluorescence spectra for global analysis of TRF using sequential and parallel excitation pathway models, respectively and EADS – evolution associated difference spectra for TA data. All plots were done in Origin 2023 (OriginLab Corp., Northampton, MA, USA).

3. Results and Discussion

3.1. Biochemical assessment of isolated phycobilisomes

The result of PBS isolation and biochemical analysis of WT- and ΔApcG-PBS are shown in **Figure 3**. In both cases, the PBS-containing blue bands were in the same interface of 0.75-1.00 M sucrose concentration (**Figure 3A**), indicating that absence of ApcG subunit does not alter the apparent PBS complex density and the general PBS subunits composition as well (**Figure 3B**).

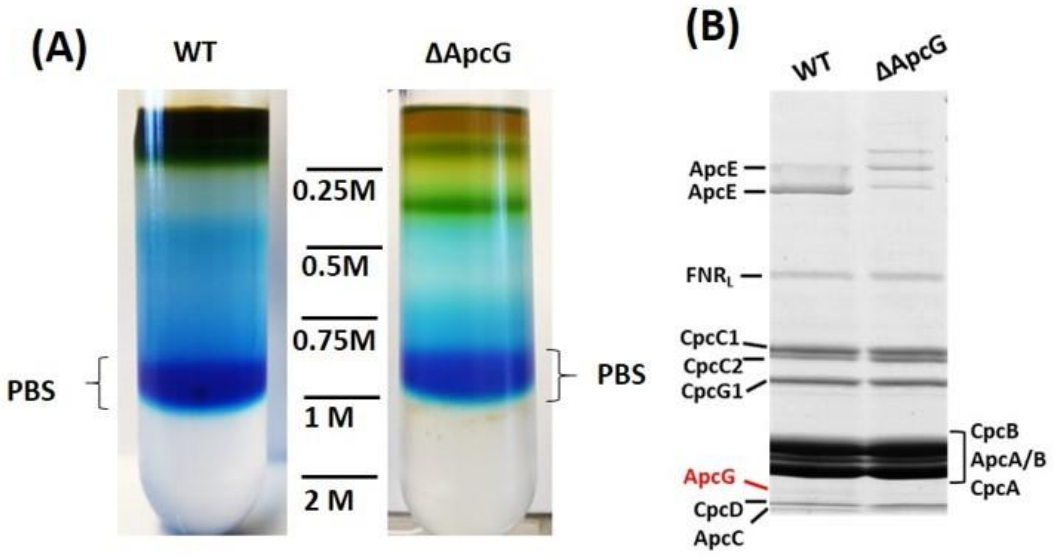

Figure 3. **Isolation and biochemical analysis of wild-type (WT) and ΔApcG-PBS.** (**A**) Sucrose density gradient ultracentrifugation isolation. The intense blue band from both strains

was used for further studies. (**B**) SDS-PAGE, 4-20% gradient gel analysis of PBS subunits. Location of ApcG (in red) is indicated.

3.2.Spectroscopic properties of ΔApcG-PBS

To determine if ApcG plays some role in the PBS assembly and excitation energy transfer within PBS, the isolated ΔApcG-PBS was studies with various spectroscopic techniques and compared with WT-PBS. Results obtained for the ΔApcG-PBS are shown in **Figure 4** (and for WT-PBS in Figure S1). **Figure 4A** (Figure S1A) presents steady-state absorption and fluorescence emission spectra of PBS recorded at 293 and 77 K. At room temperature, absorption band of the ΔApcG-PBS peaks at 621 nm (**Figure 4A**) vs 622 nm in WT (Figure S1A), which is associated with one-photon electronic transition from the ground to the first excited singlet state of phycocyanobilin (PCB) molecules bound in phycocyanin (PC) in the PBS rods. The shoulder present at the long wavelengths edge of the spectrum is due to the contributions from PCB located in allophycocyanin (APC) disks of the PBS core that peaks at ~655 nm, as indicated by local minimum of the 2nd derivative of the absorption spectrum. It seems though that our WT PBS absorption spectrum (Figure S1A) is significantly different than the one in a previous report that was used to control the ΔApcG-PBS [19].

In our experiments, for both PBSs, fluorescence emission peaks at 666 nm at 293 K. Upon freezing to 77 K, the band narrows and shifts bathochromically toward 683 nm (terminal energy emitter). It is impossible to record 77 K absorption spectrum of the ΔApcG-PBS (and other PBS as well) without compromising PBS structural integrity due to the disassembly effect of high concentration glycerol required for formation of transparent glass at low temperature. This is demonstrated in Figure S2 in which 77 K absorption spectrum and fluorescence emission spectrum of ΔApcG-PBS dispersed in 60% glycerol buffer are given. Regardless of the fact that the absorption spectrum is still quite convincing, with the main absorption band at 632 nm, associated with PC, and minor bands at 654 and 680 nm associated with the bulk of APC and the PBS core terminal energy emitter, respectively, fluorescence emission spectrum, however, is substantially altered (Figure S2A, dashed blue) in comparison to the one measured at 77 K in the plain buffer (**Figure 4A**, red line).

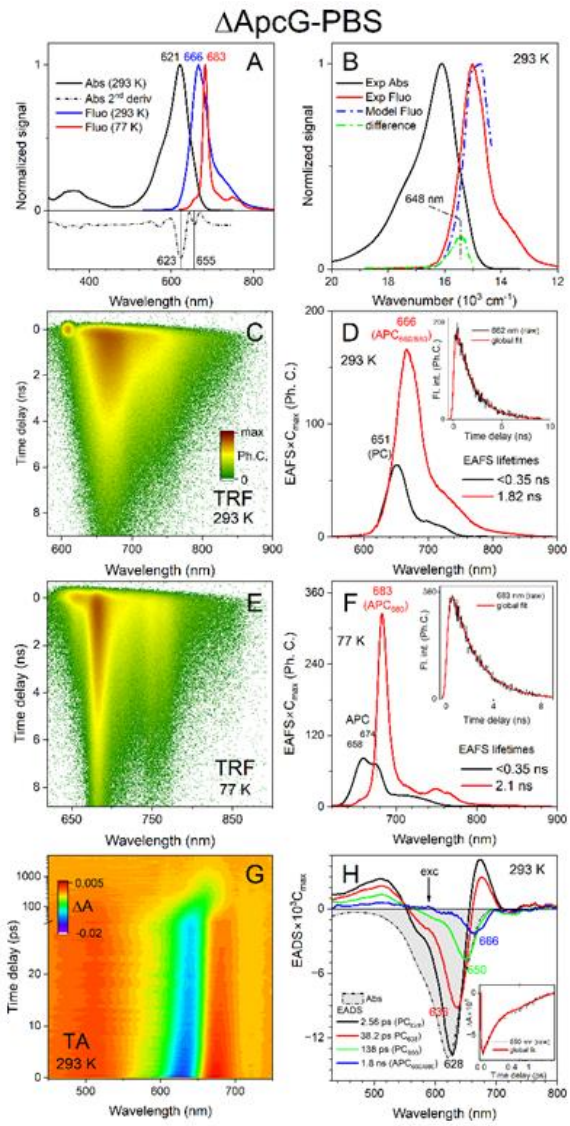

Figure 4. Spectroscopic properties of ΔApcG-PBS at 293 and 77 K. (**A**) Steady-state 293 K absorption and 293 K and 77 K fluorescence emission spectra and 2nd derivative of the absorption spectrum (arbitrary scale). The spectra are normalized at their maxima for better comparability, (**B**) Modeling of room temperature fluorescence emission from absorption spectrum based on Stepanov relation, (**C**) Pseudo-color image of time-resolved fluorescence (TRF) decay at 293 K after excitation at 610 nm, (**D**) Global analysis results (EAFS) of data from panel C, (**E**) Pseudo-color image of time-resolved fluorescence (TRF) decay at 77 K after excitation at 610 nm, (**F**) Global analysis results (EAFS) of data from panel E, (**G**) Pseudo-color image of transient absorption (TA) of PBS at 293 K after excitation at 590 nm and (**H**) Global analysis results (EADS) of TA the dataset.

It is dominated with fluorescence emission (647 nm) from PC, while signal associated with the terminal energy emitter (at 680 nm) consists only a small fraction of the whole spectrum, indicating dramatic excitation energy decoupling of PC and the PBS-core. This clearly shows that glycerol loosens interaction between PBS components. **Figure 4B** (Figure S1B) shows simplified, theoretical prediction of the expected fluorescence emission spectrum based on the experimentally obtained absorption profile at room temperature. Modeling was done with application of the Stepanov relation which assumes that Boltzmann equilibration of the excited states of fluorescing molecules occurs prior to fluorescence, and that fluorescence yield is the same across all spectral species contributing in the process [27]. Then,

$$Abs(\nu) = \frac{Fluo(\nu)}{\nu^3 C(T) e^{-\frac{h\nu}{kT}}} \quad (1)$$

where $Abs(\nu)$ and $Fluo(\nu)$ are PBS absorption and fluorescence emission profiles plotted on frequency (ν) scale, respectively, $C(T)$ is a factor that varies with temperature, k and h are Boltzmann and Planck constants respectively, and T is absolute temperature. Note that theoretical spectrum (**Figure 4B**, blue, dash-dot) appears slightly shifted to longer wavelengths compared to the experimentally obtained one (solid red). The difference between the normalized spectra reveals a band with an approximate maximum at 648 nm. This feature suggests that experimentally obtained emission profile originates not only from the energetically equilibrated pool of emitters but is also elevated from contribution brought by higher energy emitters during excitation equilibration within PBS. If so, this process should be spectrally and temporally resolvable using time-resolved fluorescence (TRF) imaging. **Figure 4C** shows pseudo-color map of the TRF image [color represents signal intensity in photon counts (Ph. C.), log scale for visibility enhancement] of the ΔApcG-PBS recorded after excitation at 610 nm at 293 K (Figure S1C, WT-PBS). The intense spot at ~610 nm around time-zero corresponds to scattering of the excitation laser beam. From visual judgement of the TRF image, it is not clear if the spectro-temporal equilibration of the fluorescence process is present or not in the data. For that purpose, the whole image was subjected to global fitting, which was done with the applications of sequential decay assuming that excitation energy unidirectionally decays to species with lower excited state energy, i.e., PC (rods) → APC (core). This type of fitting of the TRF data produces spectro-kinetic components termed as EAFS – evolution associated fluorescence spectra which,

if the model mimics the reality, should correspond to the fluorescence emission spectra of the molecular species of PCBs involved in the sequence of excitation decay. The results of the fitting are presented in **Figure 4D** (Figure S1D, WT-PBS). The EAFS profiles were corrected for maximal values of their time-dependent concentration (EAFS×C_{max}). This product more intuitively represents the true relative amplitude (but not the overall contribution) of each fluorescing component. The global fitting shows that the TRF image consists of two decay components (**Figure 4D**). The first EAFS, directly populated via excitation, decays with a lifetime value that is shorter than the width of the streak-camera response function, IRF (~0.35 ns for this time delay configuration) and populates the second component that decays with a lifetime of ~1.8 ns. The quality of fitting is highlighted in the panel insert with exemplary raw fluorescence decay trace complemented with the fitted curve from global analysis. The EAFS maxima are at 651 nm (<0.35 ns) and at 666 nm (1.82 ns). The correctness of a sequential model of the excitation decay pathway is also supported by global analysis of TRF in which unbiased parallel excitation decay (simultaneous excitation and independent decay of all spectro-kinetic components) was applied (Figure S3 for ΔApcG-PBS and Figure S4 for WT-PBS). Fast-decaying DAFS shows positive signal at shorter wavelengths and negative signal at longer wavelengths within the range of the long-lived DAFS. Such pattern suggests that the fluorescence decay at short wavelength range is associated with the simultaneous fluorescence rise in the long wavelength range which indicates excitation energy transfer from fast to slow component and directs toward sequential pathway of excitation decay. Considering EAFS positions, the faster EAFS corresponds primarily to the fluorescence of PC (PC_{650}) quenched due to excitation energy transfer to APC in the PBS core. The EAFS with maximum at 667 nm represents thermal equilibrium of APC_{660} and APC_{680} as demonstrated previously [28]. The maximum of the faster EAFS component coincides with the difference spectrum from **Figure 4B** (dash dot green) and at least partially justifies the disagreement between the experimental and hypothetical fluorescence emissions spectra. The spectral and temporal separability between two fluorescing $APC_{660/680}$ subpopulations could be achieved at 77 K at which the thermally allowable population of the APC_{660} is negligible [28]. The pseudo-color image of the fluorescence decay at 77 K is then shown in **Figure 4E** (Figure S1E, WT-PBS), with global fitting results given in **Figure 4F** (Figure S1F, WT-PBS). WT-PBS short-lived EAFS reveals single maximum at 662 nm (Figure S1F) however for ΔApcG-PBS, two local maxima at 658 and

674 nm are clearly seen (**Figure 4F**). The long-lived EAFS has a lifetime of 2.1 ns and band maximum at 683 nm and is associated with emission from APC_{680} – terminal energy emitter. The panel insert shows the representative raw TRF trace (683 nm) and the fitted curve. These results indicate that absence of ApcG causes perturbation within APC core, leading to the splitting/presence of two spectrally distinct subpopulations of the short-lived APC in comparison to spectrally homogenous APC in WT-PBS with single emission band at 662 nm (Figure S1F).

Due to the limited temporal resolution of the TRF setup, photophysical processes occurring in sub-ns scale after excitation were studied in detail with fs time-resolved (~200 fs temporal resolution) transient absorption (TA). These studies were performed only at room temperature, simply because it is impossible to freeze PBS to 77 K in the presence of glycerol as already discussed (Figure S2). The pseudo-color map of TA of ΔApcG-PBS recorded at 293 K in the 0-5 ns time delay range after excitation at 590 nm is shown in **Figure 4G** (WT-PBS in Figure S1G). The TA signal is dominated by a negative band that initially appears at ~630 nm but gradually shifts toward longer wavelengths as time delay progresses. This negative band is associated with bleaching of the ground state absorption of PCB in the PBS components (PC and APC) and is supplemented with the probe-driven stimulated emission. To further characterize the excitation migration pathways and elucidate involved spectral forms of (A)PC, the TA map was globally fitted. Considering that the 590 nm excitation primarily excites PC absorbing at shorter wavelengths, the excitation energy is then efficiently funneled through the intermediate PC species to the APC in the PBS core and finally to the PBS core terminal energy emitter(s), a sequential, unidirectional pathway model was adopted, similar to one used for TRF, however, more detailed energy transfer process should be revealed. The fitting results of TA with applications of a sequential model are usually called EADS – evolution associated difference spectra [26]. EADS of ΔApcG-PBS are shown in **Figure 4H** (Figure S1H, WT-PBS). Because PBS is an exceptionally large assembly of PCBs, excitation intensity should be set as small as possible to minimize chance of simultaneous multi-photons excitation of the individual PBS that may lead to a substantial distortion of the TA dynamics due to any potential singlet-singlet annihilation processes. Therefore, for TA experiments, excitation energy was adjusted to a value for which the longest-lived kinetic components in TA data reached a lifetime comparable to the complementary component in TRF (1.8 ns).

Global fitting demonstrated that four spectro-kinetic components are necessary to adequately reproduce TA data. For better comparability, EADS were multiplied by their C_{max}, comparably as it was done for EAFS. In addition, a scaled, reversed absorption spectrum was added as a reference. Global fitting of TA data revealed two additional spectro-kinetic components that could not be determined via TRF due to its temporal limitations of the streak camera system.

Table 1: Comparison of spectroscopic properties of ΔApcG-PBS and WT-PBS

	Abs (nm)	Fluo (nm)	TRF				TA (293 K)			
			τ_1 (ns) [λ_{max}][2] (nm)		τ_2 (ns) [λ_{max}] (nm)		τ_1 (ps)[3] (nm)	τ_2 (ps) [17] (nm)	τ_3 (ps) [17] (nm)	τ_4 (ns) [17] (nm)
			293 K	77 K	293 K	77 K				
ΔApcG-PBS	621	666, 683[1]	<0.35 [651]	<0.35 [658, 674]	1.82 [666]	2.1 [683]	2.56 [628]	38.2 [636]	138 [650]	1.8 [666]
WT-PBS	622	666, 683[1]	<0.35 [650]	<0.35 [662]	1.80 [667]	2.1 [683]	3.45 [628]	33.4 [639]	142 [651]	1.8 [663]

[1] – at 77 K, [2] – EAFS maximum, [3] – EADS minimum

Considering the position of the bleaching bands and their minima, they could be tentatively ascribed to PC_{628} (2.56-3.45 ps EADS) and PC_{636} (33.4-38.2 ps EADS), where subscripts correspond to the approximate positions of the maximum of their absorption spectra. In addition, global fitting of TA data determined the lifetime of PC_{650} of ~140 ps. It is worth noting that EADS show substantially smaller relative amplitudes in each sequential step. It suggests that regardless of low excitation intensity, singlet-singlet annihilation is unavoidable within first ~200 ps after excitation, as it will particularity manifest as a substantial drop of the amplitudes of the subsequent EADS. Consequently, to precisely determine the time constants of $PC_{628,}$ PC_{636} and PC_{650}, it will be necessary to dramatically lower the used excitation intensity, which, on the other hand, will substantially compromise signal quality [29]. Note that PC_{650} and $APC_{660/680}$ EADS are elevated by stimulated emission (SE) appearing simultaneously with true ground state absorption bleaching. This is indicated in Figure S5 which shows the superimposed complementary EADS and EAFS (Figure S5A). Because SE will be in an amplitude equal to the actual bleaching (no more photons could be stimulated to emit than were absorbed), the spectral shape of the last two EADS can be corrected for SE contributions as demonstrated in Figure S5B. The summary of all spectroscopic outcomes for both samples is provided in **Table 1**.

Listings provided in **Table 1** show that in overall there are miniscule differences between excitation dynamic characteristics in both PBS samples. This is probably because only one of the three conserved sequence motifs of ApcG [i.e., a short helix on the C-terminal domain of ApcG (ApcG-CTD)] binds in the central groove of the ApcA in two basal cylinders [17]. Absence of such structural plugin may not be able to disturb the energetic landscape of two basal cylinders where terminal energy emitters are located. These data demonstrate that from spectroscopic perspective, both types of PBSs, if incorporated to photosynthetic machinery, should comparably support photosystems in light harvesting.

3.3. State transitions analysis of WT and ΔApcG Synechocystis cells.

We demonstrated that ApcG subunit has a minimal influence on the spectroscopic properties of two purified PBS, especially on the temporal and spectral properties of the terminal energy emitter. It seems that ApcG-CTD may be anchored to the PBS, but large N-terminal domain (NTD) is left outside of PBS (ApcG-NTD) for some other functions, e.g., using structural mass spectrometry we have reported that ApcG is in the structural proximity of PB loop and comprise a structural protrusion towards the thylakoid membrane where RCs are located [30]. We hypothesize that the CTD of ApcG, together with PB-loop fine-tunes the spatial interaction of PBS with photosystems and absence of ApcG may affect the excitation energy transfer or participation in a so-called state transition process.

The mechanism of state transitions in PBS-containing photosynthetic organisms was first described back in 1960s and is characterized by two stages called State I and II [31]. Initially, it was believed that State I is present if excitation energy of absorbed light is preferentially directed to PSII, and State II corresponds to a situation for which PSI is prioritized. The transition between the two states is triggered by specific illuminations of photosystems [32] that creates an imbalance in the electron transport chain, which must be spectroscopically rebalanced by PSs [33]. The transition states are typically characterized by measuring the PSII/PSI fluorescence ratio in steady-state fluorescence emission spectrum [34], which is higher in State I than in State II. For cyanobacterium *Synechocystis* 6803, used in this work, the state transition was elaborated in details [35-38]. The overall picture from those investigations is that for a long time there was no clear consensus on the molecular mechanism(s) responsible for the observed spectroscopic changes (PSII/PSI fluorescence ratio) between states and few concurrent models were introduced

to explain the observed spectral changes. The first model, PBS-mobile, assumed that PBSs move between PSI/II photosystems changing effective absorption cross section of either photosystem. In State II, PBSs are dominantly attached to PSI (higher PSI fluorescence) and in State I more to PSII (higher PSII fluorescence) [15, 39]. Second model, called PBS-detachment/decoupling model, considers light-induced detachment of PBS from photosystems [40-42]. Third model, so-called spillover, assumes light-induced migration of both photosystems along photosynthetic membrane that affects direct excitation energy transfer (EET) (spillover) from PSII to a neighboring PSI. Larger EET (larger spillover) is in State II (EET quenches PSII fluorescence) than in State I [43]. Finally, the last model, called PSII-quenching model, and currently most preferred, assumes excitation energy quenching within inner CP47 and CP43 antenna complexes of PSII [44]. Moreover, majority of studies performed on *Synechocystis* cells assumed that absolute fluorescence intensity of PSI does not change between state transition. It was demonstrated many times by incorporating independent fluorescence marker [35, 36, 45]. Consequently, currently it is a standard practice to compare fluorescence emission spectra of whole cells in both transition states by normalizing the spectra at maximum of PSI emission [41, 45, 46].

In this study, we applied the following analysis of state transition. First, we avoided flash freezing of the samples to lock cells in either transition state. Instead, the samples, prior converted to State I and II were slowly frozen in cryostat in liquid nitrogen vapor, method that seems to be more friendly for PBSs which do not show any signs of structural disintegration. Subsequently, the TRF imaging was performed on the frozen cells in State I and II followed by spectro-kinetic analysis of the results. Generally, this study is comparable in methodology to the recent time-resolved fluorescence imaging of whole cells in State I and II of WT, ΔApcD and ΔApcF mutant strains of *Synechocystis*, performed at room temperature and *Synechococcus elongatus* 7942 at 77 K [44, 47], though we applied different global fitting model on TRF data. The experiments were done for two excitation wavelengths: 410 nm – primarily exciting Chls in PSI/II and minimally PBS and 610 nm - primarily exciting PBS and minimally Chls. The 410 nm excitation is useful to determine if PSI/II response to state transition is comparable in both strains so there is no unaccounted bias when results from more interesting 610 nm excitation are evaluated. Pseudo-color fluorescence decay images after excitation at 410 nm (primarily PSI/PSII), of WT and ΔApcG mutant *Synechocystis* cells, dark-adapted (State II) and after

illumination with far-red light in the presence of DCMU (State I) are shown in Figure S4. Global analysis of TRF maps was performed with application of model of sequential decay of excitation [26]. In all cases only two spectro-kinetic components (~300 ps and ~1 ns EAFS) were required for successful data fitting. For better comparability, the EAFS were normalized at their maxima. The profiles are dominated by the band associated with fluorescence emission of PSI, which in the fast EAFS is located at 721 nm and shifts to 728 nm in the slower EAFS, demonstrating energetic equilibration of fluorescing Chls species. The 664 nm band present in the slower component is associated with fluorescence from PBS and origins from residual direct excitation of PBS. The 689 nm (fast EAFS) and 697 nm (slow EAFS) bands are associated with fluorescence from inner antenna of PSII, CP43/47. As expected, in State I, the ratio of 697 and 728 bands (0.11) is higher compared to State II (0.06) though the band ratio is essentially the same for WT and mutant cells (in the same transition state). It demonstrates that upon direct excitation of Chls in PSI/II the spectroscopic responses to state transition are basically comparable in both strains. Consequently, any differences between strains observed in results from 610 nm excitation should be directly related with PBS and its interaction with PSI/PSII. Pseudo-color fluorescence decay images after excitation at 610 nm (PBS), of WT and ΔApcG mutant *Synechocystis* cells, dark-adapted (State II) and after illumination with far-red light in the presence of DCMU (State I) are shown in **Figure 5**. In all cases, the TRF images (**Figure 5A**, **B**, **E**, **F**) show three bands are associated with fluorescence emission from PBS, PSII and PSI respectively.

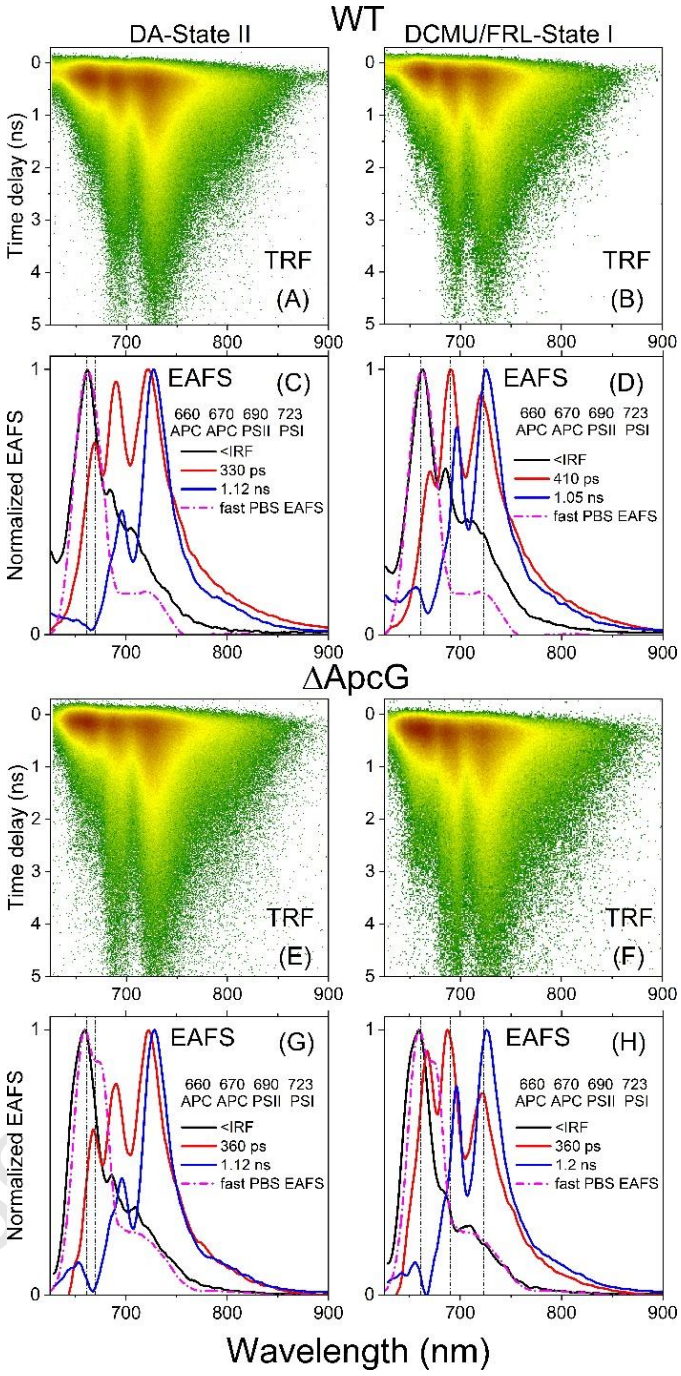

Figure 5. State transitions of WT and ΔApcG mutant *Synechocystis* cells monitored with time-resolved fluorescence (TRF) under 77 K. (**A**, **B**, **E**, **F**) Pseudo-color fluorescence decay images of cells after excitation at 610 nm, (**C**, **D**, **G**, **H**) global analysis results (EAFS) according to sequential model. DA – dark-adapted, FRL – far-red light, EAFS – evolution associated fluorescence spectra, IRF – width of instrument response function, PSI/II – photosystem I/II, APC – allophycocyanin, PBS - phycobilisome. All EAFS profiles were smoothed for clarity and are normalized for better comparison.

It is nearly impossible to evaluate changes in these profiles only based on their appearance and to obtain more insights on the spectroscopic and dynamic variations, each profile was then subjected to global analysis, as shown in **Figure 5C**, **D**, **G** and **H**. Because the goal was to determine spectro-temporal differences between two states, for fitting purpose, we have used simple unidirectional, irreversible sequential model with longer lifetimes in each step [26]. This model does not necessarily mimic true pathways of excitation migration in PBS-PSII-PSI assembly, since, as in principle, it rather shows spectral evolution of fluorescing systems, but we think it is adequate to reveal expected differences. Our global fitting required three EAFS components for a satisfactory fitting in all cases. For clarity, the EAFS profiles were smoothed and normalized in amplitude. First EAFS (**Figure 5C-D**, **G-H**, solid black) with lifetime shorter than instrument resolution (IRF width ~260 ps for 5 ns time-window) consists of sharp band with maximum at 660 nm. This band perfectly overlaps with the short-lived PBS EAFS (fast PBS EAFS, purple), though for WT, it is elevated with the scattered excitation light (**Figure 5C-D**). Therefore, it is exclusively associated with the fluorescence from APC660. This undoubtedly shows that PBSs in the frozen cells are structurally intact, otherwise, fluorescence band at 650 nm associated with PC650 (energetically uncoupled PC rods) will be evident. In addition, absence of APC680 fluorescence band, i.e., ~683 nm, PBS terminal energy emitter (**Figure 4A**, S1A vs **Figure 5A-B**) suggests very efficient energetic coupling between PBS and PSs (complete quenching due to efficient EET from the former to the latter). Note that if there is even a small fraction of uncoupled PBS, strong and long-lived fluorescence of PBS terminal energy emitter will be clearly distinguishable in the image, as demonstrated in a recent study of cells of *Synechocystis* PSII-deficient mutant [48]. It is also worthy of notice that because the first EAFS profile perfectly traces short-lived EAFS of the purified PBS, the chosen 610 nm illumination source in our experiment exclusively excites PBS and essentially there is no background signal from the unintentional direct excitation of Chl *a* in PSs. Decay of this EAFS is associated with the formation of EAFS components with three fluorescence bands at 670, 690 and 723 nm (**Figure 5C-D, G-H**). The 690 and 723 nm bands are associated with the fluorescence emission of Chl *a* in PSII and PSI respectively. The 670 nm emission bands, originated from PBS, is associated with APC670. Note that there is no indication of this spectral form in 77 K TRF of the biochemically purified PBS (**Figure 4E**, Figure S1E), suggesting it could result from two spectrally slightly different forms, structurally induced heterogeneity of APC680 upon binding of

PBS to PS interface. It seems to be in line with a recent modelling of 77 K TRF of PBS-PSI system using cells of PSII-deficient *Synechocystis* in which APC674 and APC680 were included in the modelling [48]. Please also note, in *Synechocystis* 6803, there are two types of PBSs, CpcG1-PBS and CpcL-PBS that emits at 671 nm under 77K [49]. This is an APC-less type of PBS that supposedly transfers excitation energy to PSI [50-52]. At this point, there is no indication that excitation of PSI-bound Chls is associated with PSII↔PSI spillover, as this process would require additional time and would also require prior excitation of either PSII or PSI which was not observed. The second EAFS evolves to the longest-lived, which contains only PSII and PSI emissive bands, indicating that APC670 was quenched by excitation energy transfer to PS-bound Chls. The spectral shapes of the second and third EAFS clearly demonstrate that there is some redistribution of the excitations on PSII during state transition, as the ratio of PSII and PSI emission band amplitudes are altered in both WT and mutant cells (**Figure 5C-D, G-H,** blue). Interestingly, the amplitude of the APC670 is also affected in both state II and state I, particularly in the mutant cells (**Figure 5G**, purple). It should be noticed that for both cyanobacteria strains, the effective dynamics of equivalent EAFS are comparable in State I and State II, which indicates that the fluorescence dynamics are not altered by state transition. Similar observation was also seen in the above-mentioned TRF studies of *Synechocystis* and *Synechococcus* whole cells in the literature [44, 47].

More precise comparison of the spectral shapes of the complementary EAFS (State I vs State II) by applying the following mathematical operations. The TRF maps from **Figure 5** were used to construct steady-state fluorescence emission spectra by time-integrating the TRF spectra. Subsequently, the expected steady-state emission spectra were normalized at maximum of PSI band and State I and State II were plotted (**Figure 6**, Fluo - State I, II). On the other hand, a steady-state spectrum is simply a sum of all EAFS, adjusted for their overall contributions in the TRF profiles [26]. This type of plotting highlights any net changes in the equivalent EAFS for both transition states (**Figure 6)**. Note that summing up of all those EAFS (Σ EAFS) almost perfectly reconstructs, as expected, the steady-state emission profiles (Fluo).

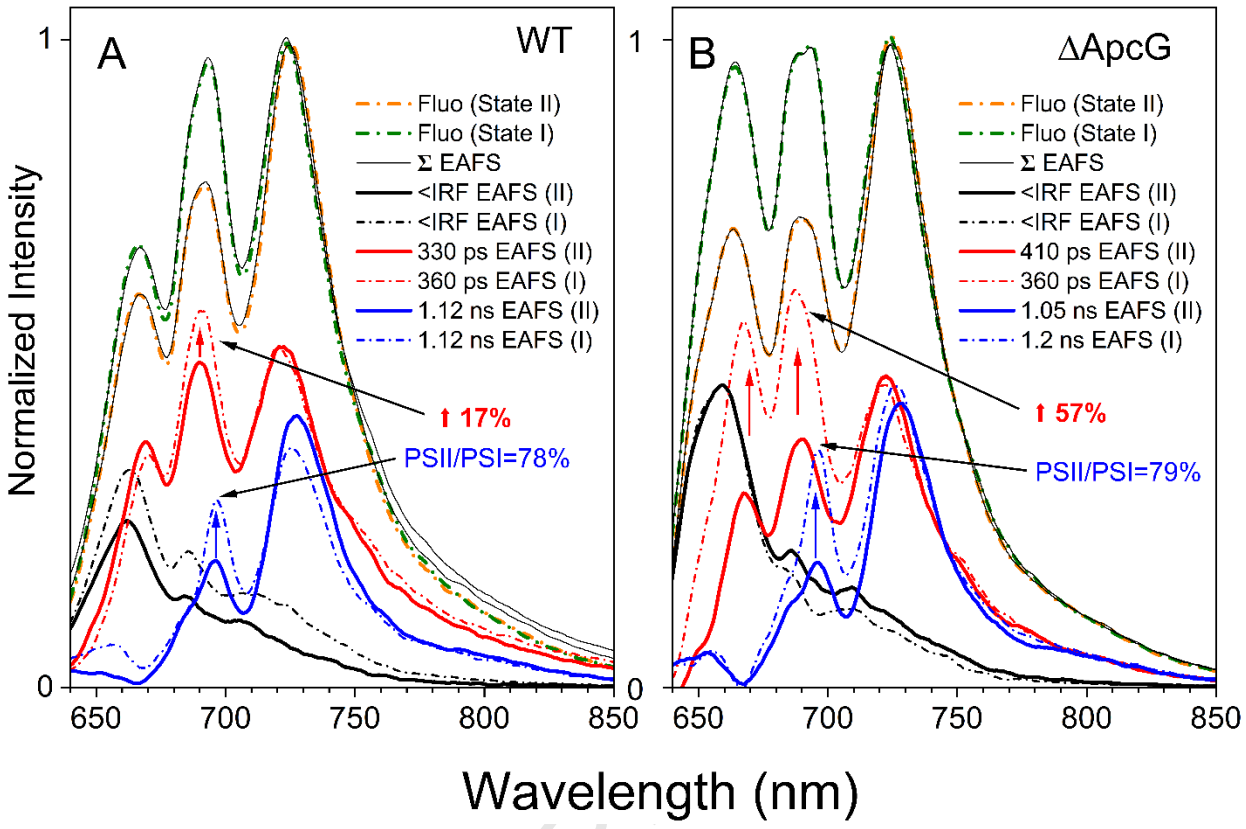

Figure 6. **Comparison of steady-state fluorescence emission spectra and global analysis components of TRF (EAFS) of whole cells of both WT (A) and ΔApcG (B) strains in State I and II.** The steady-state spectra are normalized at maximum of PSI emission band and EAFS are adjusted to levels for which their sums mimic steady-state emission spectra. Vertical arrows highlight trends in changes of signal amplitude, signal rise is also denoted as % change. For more details about the spectral reconstruction procedure refer to Figure S7 and accompanying supplementary text.

Such comparison reveals a few interesting points. It is evident that the intensity of the fluorescence band associated with emission from the PSI-bound only Chls does not change in complementary, State I – State II EAFS (for example, solid red vs dash-dot red lines, **Figure 6**) and it is true for both strains. This indicates that state transition does not involve any spillover-like process between photosystems. Significant degree of energy spillover from PSII to PSI may occur since it has been independently reported from several labs [31, 53-55]. However, our data show it is unlikely that the spillover mechanism is involved in the state transition *per se*. A similar conclusion was reached from a recent TRF study on state transitions of whole cells of *Synechococcus elongatus* [44]. Moreover, if we compare the longest-lived EAFS from both

bacterial strains in the same transition state (**Figure 6**, blue lines) it reveals that the pairs are essentially identical with no measurable relative changes in PSII and PSI emission intensities, indicating that ΔApcG does not affect state transition if it is defined purely in terms of the ratio of PSII/PSI fluorescence emission intensity. On the other hand, upon transitioning from State II to State I, ΔApcG cells give ~60% positive change (peaking at 688 nm) vs ~17% (peaking at 689 nm) in WT in the second EAFS (**Figure 6**, red solid vs red dash-dot), which is associated with the rise of the fluorescence emission starting from APC670, probably APC680 or PSII itself which seem very complex to interpret. This dramatic increase could arise from the uncoupled PBS terminal energy emitter or more PBS coupled energy to PSII (mostly CP43). The first scenario seems unlikely since any uncoupled PBS (to PSII) should have fluorescence around 683 nm, which was not observed (**Figure 6**). However, dramatic elevated 670 nm level in ΔApcG cells (State II) seemingly supports there is some PBS population emitting in this region, but its energetic coupling to terminal energy emitter is absent, since the 683 nm is absent. It seems that the second EAFS (peaking at ~690 nm) is more related to the increased energy coupling between PBS and PSII in State 1 in ΔApcG cells. ApcG-CTD is buried within two basal cylinders of PBS, deletion of it (or ApcG), however, has miniscule impacts on both purified PBS samples, indicating its non-essential structural role in PBS assembly. We tend to think ApcG-CTD only functions as a structural anchor, allowing the ApcG-NTD acting as a whipping domain involved in interactions with PSII. Absence of this spatial whipping barrier, two PBS basal cylinders tend to bind tighter to PSII in ΔApcG cells, subsequently increase the second EAFS. Nevertheless, this is the major contributor to change in the steady-state spectrum seen in the mutant strain in State I.

Note that there is a substantial difference in amplitude of the fastest EAFS emission associated with core APC (**Figure 6**, black lines in WT and ΔApcG cells respectively). In mutant, the peak 659 nm is much higher than the 662 nm in WT and is also clearly reflected in the steady-state emission (**Figure 6**, dashed green). Considering that the number of the pigments in the PBS core is constant and the fluorescence lifetime of this band seems to be comparable in both strains, the differences most likely originate from higher fluorescence quantum yield of APC in the mutant PBS (that will also include APC670) and this change could be due to the mutation-altered pigment environment that enhances the radiative decay route Note that for the isolated WT- and

ΔApcG-PBS, we indeed observed a slight split of the short-lived EAFS 662 nm peak (WT) to two peaks of 658 and 674 nm in ΔApcG-PBS (**Figure 4F**). We hypothesize that once there is PBS emission acceptor in fixed donor-acceptor stoichiometry (as PBS-PSII/I in whole cells), changes of donor fluorescence yield (ΔApcG-PBS core), becomes apparent. We consider this is the evidence showing that photosystems coupling to PBS through the linker protein, ApcG, and PB-loop as well could also affect or magnify the fluorescence features of PBS. We would like to emphasize that this hypothesis is probable only if PBS/PSII/PSI ratio remains constant in both cyanobacterial strains. The TRF data upon excitation at 410 nm demonstrate that PSII/PSI fluorescence emission ratio is the same in complementary whole cells spectra, indicating that the photosystems stoichiometry is the same. This is even clearer visualized in comparison of the steady-state fluorescence emission spectra (Figure S8). In regard to PBS, comparison of absorption spectra of both strains (Figure S9) indicates that ΔApcG cells produce ~8% more PBS therefore PBS/PS ratio will be slightly elevated in this strain however it is hard to imagine that it could be solely responsible for such dramatic spectral changes observed in fluorescence emission spectra.

At this point, it could be speculated about the origins of the changes in PSII emission band in State I vs State II in **Figure 6**. Note that there is a substantial drop (%) in the PSII emission band between the second and the third, longest-lived EAFS (between red and blue profiles), but this is not the case for the PSI band, the intensity of which essentially does not change once fluorescence evolves in time (it is particularly well seen for the mutant). The initial fluorescence band of PSII (~690 nm), as seen in the second EAFS, indicates that the excitation energy transfer from the attached PBSs statistically populates "bulk" pool of Chls distributed within the inner antenna complexes, CP43 and CP47, of PSII. The "bulk" population will split between, (I) being trapped to PSII reaction center (RC) that will cause loss of fluorescence intensity and (II) being relaxed to low energy traps within antennas that at 77 K will be more prone to long-lived fluorescence than transferring excitation to RC (up-hill energy transfer halts at 77 K). The fact that the PSII fluorescence band in State I is localized at 696 nm (**Figure** 6, blue EAFS) indicates that this extra emission is mostly associated with the fluorescence from Chl excitation traps within CP47 inner antenna [56]. Therefore, in State II, bulk of the initially excited Chls is quenched by PSII RC while in State I, a substantial portion is preferentially

trapped within CP47 (**Figure 6**). Note that for PSI-related emission, the band that is seen in the intermediate EAFS (red profiles in **Figure 6**) is already associated with the emission from deep excitation traps. Due to a large energetic gap between the energy of traps and absorption of PSI RC, any excitation energy transfer from this pool of Chls is not expected at 77 K. Consequently, the emission band should initially slightly shift toward longer wavelengths without significant change in intensity, resolving into additional energetic equilibration and the intrinsically decay, as is exactly seen (**Figure 6**, red vs blue). It is an additional indication that spillover of excitation from PSII to PSI upon transition from State I to State II is nonexistent. From this perspective state transition should be rather interpreted as some photochemical features of PSII RC itself, which hinder excitation trapping abilities of RC. All these together points out toward a PSII center quenching model of state transition, as recently promoted as the most-probable mechanism that enables the regulations of the so-called light-induced state transitions in cyanobacteria [47], which, however, cannot be investigated in details due to its nature only with application of time resolved fluorescence spectroscopy. Recent report also supports that the redox state of PSII may dictate a fast component excitation quenching process [57].

4. Conclusions

Steady-state and time-resolved spectroscopic characterization of the isolated WT and ΔApcG-PBS demonstrated the absence of ApcG, a small PBS linker peptide, has miniscule effect on the PBS structure in terms of its photophysical properties. Time-resolved fluorescence imaging of the whole cells of both strains in State I and II revealed that ApcG deletion does not alter or inhibit state transitions if it is strictly interpreted as a relative change of PSII and PSI fluorescence emission intensity. On the other hand, upon transition to State I, the mutant cells show a substantial but very short-lived (sub-ns time scale) increase of ΔApcG-PBS-related fluorescence, indicating some structural rearrangements on the interface of PBS and PSII upon PBS and PSII assembly. We hypothesize that the C-terminal α-helix of ApcG does not play important structural roles in the PBS itself assembly, rather, by anchoring to PBS through this domain, the intrinsically disordered N-terminal region might negatively reduce the structural PBS-to-PS coupling in State I in WT cells, which, however, is not yet adequate to disturb the overall PBS-to-PS excitation energy transfer process. In addition, the overall outcomes support some recent ideas of state transition as a process exclusively associated with light induced quenching within PSII only, without any involvement of inter-PS spillover.

CRediT authorship contribution statement.

Rupal Singh Tomar: Investigation, Methodology, Formal analysis, Visualization, Writing – original draft; **Dariusz M. Niedzwiedzki:** Conceptualization, Methodology, Formal analysis, Visualization, Writing – original draft; **Haijun Liu:** Conceptualization, Project administration, Funding acquisition. All participated in discussion.

Acknowledgments:

We thank Dr. Diana Kirilovsky for productive discussion and critical reading this manuscript. D.M.N. acknowledges the Center for Solar Energy and Energy Storage at McKelvey School of Engineering at Washington University in Saint Louis for finanacial support. This research is supported by the U.S. Department of Energy (DOE), Office of Basic Energy Sciences, Photosynthetic Systems (PS) Program (Grant DE-FG02-07ER15902 to H.L.).

Declarations:

The authors have no competing interests to declare that are relevant to the content of this article.

Data availability:

Data will be made available on request.

References

[1] B.A. Whitton, Diversity, ecology, and taxonomy of the cyanobacteria. In: Mann N.H., Carr N.G., editors. Photosynthetic Prokaryotes. , Plenum Press; New York, NY, USA (1992) 1–51.
[2] N Lang-Yona, A.T Kunert, L Vogel, C.J Kampf, I Bellinghausen, J Saloga, A Schink, K Ziegler, K Lucas, D. Schuppan, Fresh water, marine and terrestrial cyanobacteria display distinct allergen characteristics, Sci. Total Environ 612 (2018) 767–774.
[3] A. Glazer, Light harvesting by phycobilisomes, Annu Rev Biophys Biophys Chem 14 (1985) 47–77.
[4] E. Gantt, S.F. Conti, Phycobiliprotein localization in algae, Brookhaven Symp Biol 19 (1966) 393-405.
[5] N. Adir, Elucidation of the molecular structures of components of the phycobilisome: reconstructing a giant, Photosynth Res 85 (2005) 15-32.
[6] L.N. Liu, X.L. Chen, Y.Z. Zhang, B.C. Zhou, Characterization, structure and function of linker polypeptides in phycobilisomes of cyanobacteria and red algae: an overview, Biochim Biophys Acta 1708(2) (2005) 133-42.
[7] N. Adir, S. Bar-Zvi, D. Harris, The amazing phycobilisome, Biochim Biophys Acta Bioenerg. 1861 (2020) 148047.

[8] L. Zheng, Z. Zheng, X. Li, G. Wang, K. Zhang, P. Wei, J. Zhao, N. Gao, Structural insight into the mechanism of energy transfer in cyanobacterial phycobilisomes, Nat Commun 12 (2021) 5497
[9] S.F. Sui, Structure of Phycobilisomes, Annu Rev Biophys 50 (2021) 53-72.
[10] V. Capuano, A.S. Braux, N. Tandeau de Marsac, J. Houmard, The "anchor polypeptide" of cyanobacterial phycobilisomes. Molecular characterization of the Synechococcus sp. PCC 6301 apce gene, J Biol Chem 266(11) (1991) 7239-47.
[11] N.N. Niu, L. Lu, P.P. Peng, Z.J. Fu, D. Miao, M. Zhou, D. Noy, K.H. Zhao, The phycobilisome core-membrane linkers from Synechocystis sp. PCC 6803 and red-algae assemble in the same topology, Plant J 107(5) (2021) 1420-1431.
[12] D.V. Zlenko, I.V. Elanskaya, E.P. Lukashev, Y.V. Bolychevtseva, N.E. Suzina, E.S. Pojidaeva, I.A. Kononova, A.V. Loktyushkin, I.N. Stadnichuk, Role of the PB-loop in ApcE and phycobilisome core function in cyanobacterium Synechocystis sp. PCC 6803, Biochim Biophys Acta Bioenerg 1860(2) (2019) 155-166.
[13] P.P. Peng, L.L. Dong, Y.F. Sun, X.L. Zeng, W.L. Ding, H. Scheer, X. Yang, K.H. Zhao, The structure of allophycocyanin B from Synechocystis PCC 6803 reveals the structural basis for the extreme redshift of the terminal emitter in phycobilisomes, Acta Crystallographica Section D-Structural Biology 70 (2014) 2558-2569.
[14] C. Dong, A. Tang, J. Zhao, C.W. Mullineaux, G. Shen, D.A. Bryant, ApcD is necessary for efficient energy transfer from phycobilisomes to photosystem I and helps to prevent photoinhibition in the cyanobacterium Synechococcus sp. PCC 7002, Biochim Biophys Acta 1787(9) (2009) 1122-8.
[15] M.K. Ashby, C.W. Mullineaux, Cyanobacterial ycf27 gene products regulate energy transfer from phycobilisomes to photosystems I and II, FEMS Microbiol Lett 181(2) (1999) 253-60.
[16] L. Zheng, Z. Zheng, X. Li, G. Wang, K. Zhang, P. Wei, J. Zhao, N. Gao, Structural insight into the mechanism of energy transfer in cyanobacterial phycobilisomes, Nat Commun 12(1) (2021) 5497.
[17] M.A. Domínguez-Martín, P.V. Sauer, H. Kirst, M. Sutter, David Bína, Basil J. Greber, Eva Nogales, T. Polívka, C.A. Kerfeld, Structures of a phycobilisome in light-harvesting and photoprotected states, Nature 609 (2022) 835-845.
[18] H. Liu, Cyanobacterial Phycobilisome Allostery as Revealed by Quantitative Mass Spectrometry, Biochemistry 62 (2023) 1307-1320.
[19] R. Espinoza-Corral, M. Iwai, T. Zavřel, S. Lechno-Yossef, M. Sutter, J. Červený, K.K. Niyogi, C.A. Kerfeld, Phycobilisome protein ApcG interacts with PSII and regulates energy transfer in Synechocystis, Plant Physiology (2023) kiad615.
[20] M. Angeleri, D. Muth-Pawlak, E.M. Aro, N. Battchikova, Study of O-Phosphorylation Sites in Proteins Involved in Photosynthesis-Related Processes in Synechocystis sp. Strain PCC 6803: Application of the SRM Approach, J Proteome Res 15(12) (2016) 4638-4652.
[21] M.M. Allen, Simple Conditions for Growth of Unicellular Blue-Green Algae on Plates(1, 2), J Phycol 4(1) (1968) 1-4.
[22] H. Liu, D.A. Weisz, M.M. Zhang, M. Cheng, B. Zhang, H. Zhang, G.S. Gerstenecker, H.B. Pakrasi, Michael L. Gross, R.E. Blankenship, Phycobilisomes Harbor FNRL in Cyanobacteria, Molecular Biology and Physiology 10 (2019) e00669-19.
[23] A.N. Glazer, Phycobiliproteins, Methods Enzymol 167 (1988) 291-303.
[24] D.M. Niedzwiedzki, N.C.M. Magdaong, X. Su, H. Liu, Biochemical and spectroscopic characterizations of the oligomeric antenna of the coral symbiotic Symbiodiniaceae *Fugacium kawagutii*, Photosynthesis Research (2022).
[25] D.M. Niedzwiedzki, M. Fuciman, H.A. Frank, R.E. Blankenship, Energy transfer in an LH4-like light harvesting complex from the aerobic purple photosynthetic bacterium *Roseobacter denitrificans*, Biochim Biophys Acta 1807(5) (2011) 518-28.

[26] I.H.M. van Stokkum, D.S. Larsen, R. van Grondelle, Global and target analysis of time-resolved spectra, Biochimica et Biophysica Acta (BBA)-Bioenergetics 1657(2–3) (2004) 82–104.
[27] B.I. Stepanov, A universal relation between the absorption and luminescence spectra of complex molecules, Sov. Phys. Dokl. 2 (1957) 81-84.
[28] V.I. Stadnichuk, E.P. Lukashev, M.F. Yanyushin, D.V. Zlenko, E.M. Muronez, I.N. Stadnichuk, P.M. Krasilnikov, Energy transfer pathways among phycobilin chromophores and fluorescence emission spectra of the phycobilisome core at 293 and 77 K, Dokl Biochem Biophys 465(1) (2015) 401-405.
[29] I.H.M. van Stokkum, M. Gwizdala, L. Tian, J.J. Snellenburg, R. van Grondelle, H. van Amerongen, R. Berera, A functional compartmental model of the Synechocystis PCC 6803 phycobilisome, Photosynthesis Research 135 (2018) 87-102.
[30] H. Liu, AlphaFold and Structural Mass Spectrometry Enable Interrogations on the Intrinsically Disordered Regions in Cyanobacterial Light-harvesting Complex Phycobilisome, J Mol Biol 434(21) (2022) 167831.
[31] N. Murata, Control of excitation transfer in photosynthesis. I. Light-induced change of chlorophyll a fluorescence in Porphyridium cruentum, Biochim Biophys Acta 172(2) (1969) 242-51.
[32] N.K. Singh, R.R. Sonani, R.P. Rastogi, D. Madamwar, The phycobilisomes: an early requisite for efficient photosynthesis in cyanobacteria, EXCLI J 14 (2015) 268-289,.
[33] H. Liu, H. Zhang, D.M. Niedzwiedzki, M. Prado, G. He, M.L. Gross, R.E. Blankenship, Phycobilisomes Supply Excitations to Both Photosystems in a Megacomplex in Cyanobacteria, Science 342 (2013) 1104-1107.
[34] P.I. Calzadilla, D. Kirilovsky, Revisiting cyanobacterial state transitions, Photochem. Photobiol. Sci 19 (2020) 585.
[35] P.I. Calzadilla, J. Zhan, P. Sétif, C. Lemaire, D. Solymosi, N. Battchikova, Q. Wang, D. Kirilovsky, The Cytochrome b6f Complex Is Not Involved in Cyanobacterial State Transitions, The Plant Cell 31 (2019) 911–931.
[36] D.V. Zlenko, I.V. Elanskaya, E.P. Lukashev, Y.V. Bolychevtseva, N.E. Suzina, E.S. Pojidaeva, I.A. Kononova, A.V. Loktyushkin, I.N. Stadnichuk, Role of the PB-loop in ApcE and phycobilisome core function in cyanobacterium Synechocystis sp. PCC 6803 Biochimica Biophysica Acta (BBA)Bioenergetics 1860 (2019) 155-166.
[37] J. Zhao, L. Chen, F. Gao, Q. Wang, Z. Qiu, W. Ma, Identification of biochemical association of phycobilisome with photosystems in cyanobacterial state transition, Acta Biochimica et Biophysica Sinica 46 (2014) 911 - 916.
[38] A.M. Acuña, P. van Alphen, F. Branco dos Santos, R. van Grondelle, K.J. Hellingwerf, I.H.M. van Stokkum, Spectrally decomposed dark-to-light transitions in Synechocystis sp. PCC 6803, Photosynth Research 137 (2018) 307–320.
[39] S. Joshua, C.W. Mullineaux, The rpaC gene product regulates phycobilisome-photosystem II interaction in cyanobacteria, Biochim Biophys Acta 1709(1) (2005) 58-68.
[40] V. Chukhutsina, L. Bersanini, E.-M. Aro, H.v. Amerongen, Cyanobacterial Light-Harvesting Phycobilisomes Uncouple From Photosystem I During Dark-To-Light Transitions, Sci Rep 5 (2015) 14193.
[41] R. Kaňa, The slow S to M fluorescence rise in cyanobacteria is due to a state 2 to state 1 transition, Biochimica et Biophysica Acta (BBA) - Bioenergetics 1817 (2012) 1237-1247.
[42] A.M. Acuña, P. van Alphen, F. Branco dos Santos, R. van Grondelle, K.J. Hellingwerf, I.H.M. van Stokkum, Spectrally decomposed dark-to-light transitions in a PSI-deficient mutant of Synechocystis sp. PCC 6803, Biochimica et Biophysica Acta (BBA) - Bioenergetics 1859(2) (2018) 57-68.
[43] J. Olive, Ultrastructure and light adaptation of phycobilisome mutants of Synechocystis PCC 6803, Biochimica et Biophysica Acta (BBA) - Bioenerge 1319 (1997) 275-282.
[44] R.R. Choubeh, E. Wientjes, P.C. Struik, D. Kirilovsky, H. van Amerongen, State transitions in the cyanobacterium

7942 involve reversible quenching of the photosystem II core, Bba-Bioenergetics 1859(10) (2018) 1059-1066.
[45] T. Ogawa, T. Harada, H. Ozaki, K. Sonoike, Disruption of the ndhF1 Gene Affects Chl Fluorescence through State Transition in the Cyanobacterium synechocystis sp. PCC 6803, Resulting in Apparent High Efficiency of Photosynthesis, Plant Cell Physiol 54 (2013) 1164–1171.
[46] K. Kondo, X.X. Geng, M.I. Mitsunori Katayama, Distinct roles of CpcG1-phycobilisome and CpcG2-phycobilisome in state transitions in a cyanobacterium Synechocystis sp. PCC 6803, Photosynth Res 99 (2009) 217–225.
[47] A.F. Bhatti, R.R. Choubeh, D. Kirilovsky, E. Wientjes, H. van Amerongen, State transitions in cyanobacteria studied with picosecond fluorescence at room temperature, Bba-Bioenergetics 1861(10) (2020).
[48] I.H.M. van Stokkum, P. Akhtar, A. Biswas, P.H. Lambrev, Energy transfer from phycobilisomes to photosystem I at 77 K, Front Plant Sci 14 (2023).
[49] D.M. Niedzwiedzki, H. Liu, R.E. Blankenship, Excitation Energy Transfer in Intact CpcL-Phycobilisomes from Synechocystis sp. PCC 6803, J Phys Chem B 123(22) (2019) 4695-4704.
[50] M. Watanabe, D.A. Semchonok, M.T. Webber-Birungi, S. Ehira, K. Kondo, R. Narikawa, M. Ohmori, E.J. Boekema, M. Ikeuchi, Attachment of phycobilisomes in an antenna-photosystem I supercomplex of cyanobacteria, Proc Natl Acad Sci U S A 111(7) (2014) 2512-7.
[51] L. Zheng, Z. Zhang, H. Wang, Z. Zheng, J. Wang, H. Liu, H. Chen, C. Dong, G. Wang, Y. Weng, N. Gao, J. Zhao, Cryo-EM and femtosecond spectroscopic studies provide mechanistic insight into the energy transfer in CpcL-phycobilisomes, Nat Commun 14(1) (2023) 3961.
[52] R. Guo, Y.L. Xu, J.X. Zhu, H. Scheer, K.H. Zhao, Assembly of CpcL-phycobilisomes, Plant J (2024).
[53] P. Akhtar, F. Balog-Vig, W. Han, X. Li, G. Han, J.R. Shen, P.H. Lambrev, Quantifying the Energy Spillover between Photosystems II and I in Cyanobacterial Thylakoid Membranes and Cells, Plant Cell Physiol 65(1) (2024) 95-106.
[54] M. Yokono, A. Takabayashi, S. Akimoto, A. Tanaka, A megacomplex composed of both photosystem reaction centres in higher plants, Nat Commun 6 (2015) 6675.
[55] K. Ifuku, Diversity of the PSI-PSII Megacomplexes That Conduct Energy Spillover in Green Plants, Plant Cell Physiol 64(8) (2023) 844-846.
[56] E.G. Andrizhiyevskaya, A. Chojnicka, J.A. Bautista, B.A. Diner, R. van Grondelle, J.P. Dekker, Origin of the F685 and F695 fluorescence in photosystem II, Photosynth Res 84(1-3) (2005) 173-80.
[57] P. Akhtar, G. Sipka, W. Han, X. Li, G. Han, J.R. Shen, G. Garab, H.S. Tan, P.H. Lambrev, Ultrafast excitation quenching by the oxidized photosystem II reaction center, J Chem Phys 156(14) (2022) 145101.